Available online at www.sciencedirect.com
ScienceDirect
Journal of Solid State Chemistry 180 (2007) 2465–2470
JOURNAL OF SOLID STATE CHEMISTRY
www.elsevier.com/locate/jssc

Structural arrangements of the ternary metal boride carbide compounds MB_2C_4 (M = Mg, Ca, La and Ce) from first-principles theory

Chang-Ming Fang[1], Joseph Bauer, Jean-Yves Saillard, Jean-François Halet*

Laboratoire des Sciences Chimiques de Rennes, UMR 6226 CNRS-Université de Rennes 1, Avenue du Général Leclerc, 35042 Rennes Cedex, France

Received 13 March 2007; received in revised form 25 June 2007; accepted 30 June 2007
Available online 7 July 2007

Abstract

The structural arrangements of the ternary metal borocarbides MB_2C_4 (M = Mg, Ca; La and Ce) are investigated using density-functional theory (DFT) calculations within the generalized gradient approximation (GGA). Results indicate that these compounds adopt a layered structure consisting of graphite-like B_2C_4 layers alternating with metal sheets. Within the hexagonal layers, the coloring with the –C–C–C–B–C–B– sequence is energetically more stable than that with the –C–C–C–C–B–B– one. The electronic structures of these compounds, mainly determined by the B_2C_4 sheets, can be rationalized with the simple valence electron distribution $M^{2+}[B_2C_4]^{2-}xe^-$, with the metals essentially acting as two-electron donors with respect to the boron–carbon network, the other x electrons remaining in the relatively narrow d and/or f bands of the metals. Accordingly, MB_2C_4 are narrow band-gap semiconductors ($\Delta E \approx 0.2$–0.4 eV) with M = Mg and Ca. On the other hand, with M = La and Ce, the compounds are conducting with a relatively high density of states at the Fermi level predominantly metal in character with substantial B/Cπ* antibonding state admixture.

Keywords: Coloring problem; Density functional theory calculations; Electronic structure; MB_2C_4 phases; Structural arrangements; Ternary metal boride carbides; Valence electron counting

1. Introduction

Many experimental works have shown that the combination of boron and carbon elements with rare-earth metals (RE) leads to the formation of numerous ternary compounds of formula $RE_xB_yC_z$ exhibiting a variety of different structural arrangements with boron–carbon sub-structures ranging from zero-dimensional units isolated from each other in a matrix of metal atoms to one- and two-dimensional networks [1–3]. The correlation between the structure of these rare-earth metal boron carbides and the electron count has been amply discussed over the last years. Indeed, it has been shown that the dimensionality and the topology of the boron–carbon sub-lattices in these compounds are strongly dependent upon the averaged valence electron concentration (VEC) per light atom (B and C). This VEC is obtained assuming an ionic bonding scheme—it is a strong approximation—between the boron–carbon network and the metal atoms considered as being fully oxidized in the following way: VEC = $(nx+3y+4z)/(y+z)$ for any compound $RE_xB_yC_z$ (n is generally 3, sometimes 4) [1–3].

Ternary compounds with a VEC slightly larger or equal to 4 generally adopt a layered structure with covalently bonded boron–carbon sheets sandwiching metal sheets. This is not surprising since it is close to 4, the VEC of graphite, a typical two-dimensional (2D) compound. Depending on the nature of the metal and the stoichiometry, different kinds of boron–carbon planar networks can be encountered. Sheets made of fused diamonds and octagons are observed in all the REB_2C_2 compounds, except in ScB_2C_2 in which the boron–carbon layers are composed of fused pentagons and heptagons [1]. Boron–carbon sheets in most of the REB_2C compounds are formed of fused diamonds and heptagons [1,4], but with Ce

*Corresponding author. Fax: +33 2 23 23 68 40.
E-mail addresses: C.Fang@science.ru.nl (C.-M. Fang), halet@univ-rennes1.fr (J.-F. Halet).
[1]Also correspondance to.

0022-4596/$ - see front matter © 2007 Elsevier Inc. All rights reserved.
doi:10.1016/j.jssc.2007.06.028

and the actinide elements Th and U (high temperature phase), planar layers consist of the assemblage of fused hexagons and nine-membered rings instead [1,4]. Finally another arrangement is observed in α-UB_2C (low temperature phase) with fused eight-membered rings [1,4]. It is worth mentioning that all these layered compounds are situated in the ternary phase diagram on the tie-line from diborides to graphites which are themselves typical 2D compounds. In addition to these well-characterized $RE B_2C_2$ and $RE B_2C$ phases, there exists at least one more layered phase on this line in the carbon-rich region, namely $RE B_2C_4$. Compounds of such a composition not only with La and Ce (VEC = 4.17) but also with alkaline-earth metal (Ca, Sr, and Ba) (VEC = 4) were first reported by Markovskii and co-workers in the mid-1960s [5,6]. Some years later, one of us could again prepare some of these phases and was able to index the X-ray powder patterns on the basis of a hexagonal unit cell with the parameters $a = 4.500$ (3) Å and $c = 9.428$ (3) Å, and $a = 4.4913$ (6) Å and $c = 9.3016$ (3) Å for LaB_2C_4 and CeB_2C_4, respectively [7]. The value of the a parameters in these compounds, slightly larger than that of graphite (4.2629 Å if a $(\sqrt{3} \times \sqrt{3})R30^\circ$ supercell is considered), strongly suggests that their structure derives from the graphitic structure with two boron atoms replacing two carbon atoms in the hexagonal graphitic sheets and metals in between. Unfortunately, no single-crystal data are available yet to confirm the boron vs. carbon distribution inside the sheets. Indeed, the single crystals obtained on the surface of compacted pellets after long heating (more than a week over 2000 °C) are very thin plates less than one μm thick. These plates hydrolyse in a moistured atmosphere and are not suitable for single-crystal X-ray analysis [7].

The question of boron vs. carbon distribution inside the sheets, termed "the coloring problem" [8], is often faced by solid-state chemists and has been tackled in particular for $M B_2C_2$ (M = alkaline- or rare-earth metal) phases [8,9] and more recently for YB_2C [10]. With two B and four C atoms to form hexagons in the light-atom 6^3 sub-lattice of $RE B_2C_4$, two simple different colorings, **I** (–C–C–C–B–C–B– sequence) and **II** (–C–C–C–C–B–B– sequence) are possible within the sheets (Fig. 1), coherent with the hexagonal (or trigonal, or at least orthorhombic pseudo-hexagonal) experimental unit cell. In both colorings, the layers A stack along the c direction in an eclipsed A–A fashion, leading to hexagonal prismatic holes, one third of which being occupied by metal atoms. With $c = 9.428$ (3) Å this allows two different possibilities to arrange the metal atoms for each coloring with metal atoms stacking along the c direction, either in zigzag (stacking A-α-A-β, **a**) or on top of each other (stacking A-α-A-α, **b**). The value of the c-axis experimentally measured for $RE B_2C_4$ (vide supra) prevents a stacking A-α-A-β-A-γ-. Therefore, four different structural arrangements were built, **Ia**, **Ib**, **IIa** and **IIb**. They are shown in Fig. 1.

A quantitative theoretical analysis at the density-functional theory (DFT) level was carried out in order to speculate on the structural preference in the phases $M B_2C_4$ (M = alkaline- and rare-earth metal). The main results are reported in this paper.

2. Computational details

Structural optimizations and electronic structure calculations were carried out using the code VASP (Vienna *ab initio* Simulation Program) [11,12] with the PAW (Projector-Augmented Waves) potentials [13,14]. The generalized gradient approximation of Perdew, Burke and Ernzerhof (GGA-PBE) [15] was employed for the exchange and correlation energy terms. The electronic wave functions were sampled on dense meshes of k points in the irreducible 2D (pseudo-hexagonal) and 3D Brillouin zones (BZ) using the Monkhorst–Pack method [16]. The cut-off energy of the wavefunctions was 850 eV. The cut-off energy for the augmented wave functions was 900 eV. Such high values were needed to get accurate cohesive energies. Convergence of the total energy with the number of the k points in the Brillouin zones and the plane wave cut-off energy was checked.

The electronic structure of the $[B_2C_4]^{2-}$ sheets was obtained in the following way. We first optimized atomic coordinates for a neutral B_2C_4 single sheet with the lattice cell parameters fixed, "isolated" from the others by a large inter-sheet distance (8 Å). The electronic structure was

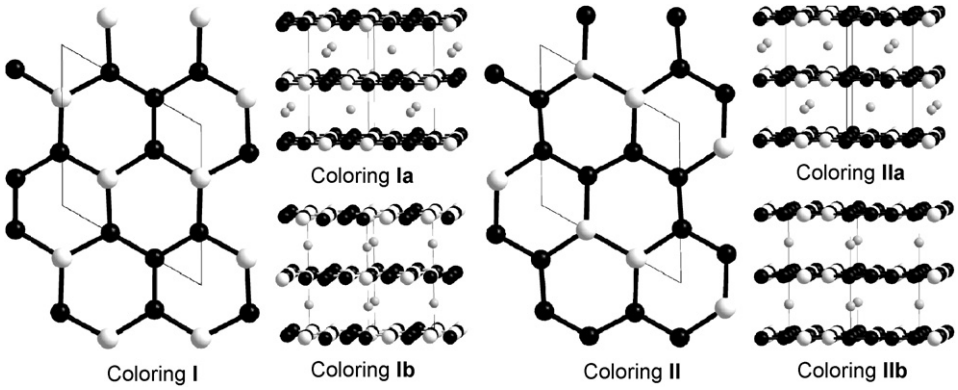

Fig. 1. Schematic representation of the $M B_2C_4$ structures. Boron, carbon and metal atoms are drawn as white, black and gray balls.

calculated for the optimized B_2C_4 sheet. The Fermi level was then shifted to the position corresponding to $[B_2C_4]^{2-}$.

3. Results and discussion

3.1. Energetics

The geometry of a two-dimensional $[B_2C_4]^{2-}$ sheet (isoelectronic to a graphite sheet) with coloring **I** and **II** was first optimized. The two optimized lattices are basically pseudo-hexagonal, with coloring **I** quite substantially preferred over coloring **II** (328 meV per formula unit (f.u.), see Table 1). The actual plane (2D space) groups of **I** and **II** are hexagonal *p*31*m* and rectangular *p*2*mm,* respectively, (the latter can be described with a primitive oblique unit cell with $a \sim b$ and $\gamma \sim 120^\circ$). Interestingly, the preferred arrangement is that where the two boron atoms are further apart (coloring **I**) rather than adjacent (coloring **II**). The same conclusions were observed for MB_2C_2 and MB_2C compounds [8–10]. The role of the metal in the structural preference was then considered. From a symmetry analysis the lattices of MB_2C_4 compounds exhibit base-centered orthorhombic supercells (the space groups are $C222_1$, *Cmcm*, *Cmcm*, and *Cmmm* for the four arrangements **Ia**, **Ib**, **IIa** and **IIb**, respectively). The relationship between the orthorhombic cells and the pseudo-hexagonal unit cells that we will use in the text is: $a_{orth} \approx a_{hex}$, $b_{orth} \approx \sqrt{3}\, b_{hex}$ and $c_{orth} = c_{hex}$. Full geometry optimizations of the four arrangements **Ia**, **Ib**, **IIa** and **IIb** shown in Fig. 1 were carried out with different metals, La, Ce, Ca, as well as Mg (MgB_2C_2 with graphitic-like boron–carbon sheets exists [17], so we could think that MgB_2C_4 may also exist). The cohesive energies estimated from the optimized structures are given in Table 1. Regardless of the metals, structures **Ia** and **Ib** are largely preferred over structures **IIa** and **IIb** by ca. 500–800 meV per f.u. Due to this large energy difference, we will limit our discussion mainly to coloring **I**-type structures.

With divalent metals (Mg, Ca) structure **Ib** with the metal atoms stacking along the *c* axis on top of each other is slightly preferred, whereas with trivalent metals (La, Ce (eventually tetravalent)), arrangement **Ia** is slightly more stable. However, the energy difference is small (<150 meV per f.u.), indicating that the structural preference in these MB_2C_4 phases is mainly governed by the boron vs. carbon distribution.

Table 1
Relative cohesive energies for different optimized MB_2C_4 structures (meV/f. u.)

	Struture **Ia**	Struture **Ib**	Struture **IIa**	Struture **IIb**
$[B_2C_4]^{2-}$	0		328	
MgB_2C_4	150	0	857	846
CaB_2C_4	29	0	701	745
LaB_2C_4	0	98	559	736
CeB_2C_4	0	101	653	749

Pertinent metrical data are given in Table 2. For a given metal, lattice parameters of the pseudo-hexagonal arrangements are nearly similar for all structures. Regardless of the metal the *a* parameter is constant, ca. 4.58 Å. On the other hand the *c* parameter strongly depends on the size of the metal (ca. 7.5 Å with Mg, 8.8 Å for Ca and 9.3–9.4 Å with La or Ce). Note that similar cell parameters for structures **Ia–b** and **IIa–b** prevent to discriminate one arrangement over another solely on the basis of metrical data. Indeed, cell parameters computed for all structures with La and Ce compare rather well with the cell parameters experimentally measured (see Table 2). The *a* parameter is computed to be slightly larger (ca. 2%), whereas the computed *c* parameter is very slightly shorter by less than 1%.

Similar *a* parameters regardless of the metal are due to the fact that the chemical bond lengths between the non-metallic elements are almost constants for all the MB_2C_4 compounds in coloring **I** with C–C distances of about 1.46 (±0.01) Å and B–C distances of about 1.56 (±0.01) Å, as shown in Tables 2a and b. The later compares well with the B–C distances measured in LiBC [18] and MgB_2C_2 [17], 1.56–1.59 Å, for instance, which contain also graphite-related layers. As in LiBC, B/C sheets are planar overall [18]. No significant deviation from planarity is observed when calculations are performed without any symmetry constraint. That is somewhat surprising as *M* atoms can be divalent (Mg and Ca), trivalent (La) or eventually tetravalent (Ce) from the ionic model point of view. As expected, the *M*–B/C bond lengths depend upon the radius of the metal ions. With Mg, the 12 *M*–B/C bonds are

Table 2a
Computed (pseudo) hexagonal lattice parameters (Å) and pertinent bond lengths (Å) (multiplicy in brackets) for the MB_2C_4 phases (M = Mg and Ca)

	Structure **Ia**	Structure **Ib**
MgB_2C_4		
a, *c*	4.5771, 7.5287	4.5745, 7.5167
B–C	1.55 (×1), 1.56 (×2)	1.55 (×1), 1.56 (×2)
C1–C	1.46 (×2), 1.47 (×1)	1.46 (×1), 1.47 (×2)
C2–C	1.47 (×1),	1.46 (×1)
C2–B	1.56 (×2)	1.56 (×2)
C3–C	1.46 (×1)	1.47 (×1)
C3–B	1.55 (×1), 1.56 (×1)	1.55 (×1), 1.56 (×1)
Mg–C	2.41 (×4), 2.43 (×2)	2.40 (×2), 2.41 (×2)
Mg–B	2.44 (×2) 2.43 (×4)	2.43 (×2), 2.45 (×2)
		2.42 (×2), 2.43 (×2)
CaB_2C_4		
a, *c*	4.5844, 8.7943	4.5843, 8.8046
B–C	1.56 (×3)	1.55 (×1), 1.56 (×1)
C1–C	1.47 (×3)	1.57 (×1)
C2–C	1.47 (×1),	1.47 (×3)
C2–B	1.56 (×2)	1.47 (×1),
C3–C	1.47 (×1)	1.56 (×2)
C3–B	1.56 (×2)	1.47 (×1)
Ca–C	2.62 (×2), 2.64 (×4)	1.55 (×1), 1.57 (×1)
	2.76 (×2)	2.64 (×6), 2.76 (×2)
–B	2.71 (×2), 2.72 (×2)	2.71 (×4)

almost identical, ca. 2.43($\pm$0.02) Å. This somewhat differs from MgB_2C_2, where the Mg–C and Mg–B distances vary from 2.25 to 2.52 Å [17]. The interatomic M–B/C distances fall in larger ranges for the compounds with larger metal ions: about 2.62–2.76 Å for Ca–B/C, 2.55–2.94 Å for La/Ce–B/C (see Tables 2a and b).

3.2. Electronic structures

Let us start considering the electronic structure of a 2D model made of one $[B_2C_4]^{2-}$ layer with colorings **I** and **II**, both isoelectronic to graphite. The energy dispersion curves associated with various crystal orbitals along the high-symmetry lines defining the irreducible part of the Brillouin zone of the pseudo-hexagonal cells are shown in Fig. 2 and compared to that of graphite. The band structure of the later has been studied in great details over the years [19]. It was computed here again using the $(\sqrt{3}\times\sqrt{3})R30^\circ$ supercell of the 2D *p6m* hexagonal system (Fig. 3) in order to compare its band structure with those of $[B_2C_4]^{2-}$ with colorings **I** and **II**. Graphite is a zero-gap semi-conductor or a semi-metal where π valence and π^* conduction bands just touch at the point Γ of the $(\sqrt{3}\times\sqrt{3})R30^\circ$ Brillouin zone (or at the K point of the Brillouin zone of pristine graphite) [19] (Figs. 2b and 3).

The result of the substitution of two C atoms by two B^- anions is the removal of the degeneracy at the point K due to the lowering of symmetry in both colorings (vide supra). This is shown in Figs. 2 and 4. The $[B_2C_4]^{2-}$ model with the coloring **I** arrangement exhibits a direct energy band gap (about 0.2 eV) at Γ. Interestingly, $[B_2C_4]^{2-}$ with coloring **II** shows a larger direct energy band gap (about 0.4 eV) in the Γ-K line. As expected, the π valence band is predominantly carbon in character, whereas the π^* conduction band shows a substantial boron character. The band gap is larger for coloring **II** than for coloring **I** probably because of the presence of B–B bonds in the former and/or for symmetry reasons. Note that the Γ-K line in the Brillouin zone corresponds to the direction with the B–B bonds in the direct space.

What is the role of the metal atoms? Comparable, if not similar results, i.e., a comparable semi-conducting behavior is expected with the divalent Mg and Ca metals. Indeed, the

Table 2b
Computed (pseudo) hexagonal lattice parameters (Å) and pertinent bond lengths (Å) (multiplicy in brackets) for the MB_2C_4 phases (M = La and Ce)

	Structure **Ia**	Structure **Ib**	Experimental [9]
LaB_2C_4			
a, c	4.5878, 9.3657	4.5791, 9.2819	4.500, 9.428
B–C	1.56 (× 3)	1.56 (× 2), 1.56 (× 1)	
C1–C	1.46 (× 2), 1.47 (× 1)	1.46 (× 1), 1.47 (× 2)	
C2–C	1.47 (× 1),	1.47 (× 1),	
C2–B	1.56 (× 2)	1.56 (× 1), 1.58 (× 1)	
C3–C	1.46 (× 1)	1.46 (× 1)	
C3–B	1.56 (× 2)	1.56 (× 2)	
La–C	2.66 (× 2), 2.70 (× 2)	2.67 (× 2), 2.74 (× 2)	
	2.78 (× 2), 2.95 (× 2)	2.83 (× 2), 2.90 (× 2),	
La–B	2.88 (× 2), 2.89 (× 2)	2.76 (× 2), 2.94 (× 2)	
CeB_2C_4			
a, c	4.5819, 9.3724	4.5773, 9.3055	4.4913, 9.3016
B–C	1.56 (× 3)	1.55 (× 1), 1.58 (× 2)	
C1–C	1.47 (× 3)	1.47 (× 3)	
C2–C	1.47 (× 1),	1.47 (× 1),	
C2–B	1.56 (× 2)	1.55 (× 2)	
C3–C	1.47 (× 1)	1.47 (× 1)	
C3–B	1.56 (× 2)	1.55 (× 1), 1.58 (× 1)	
Ce–C	2.55 (× 2), 2.63 (× 2)	2.58 (× 2), 2.62 (× 2)	
	2.66 (× 2), 2.86 (× 2)	2.71 (× 2), 2.85 (× 2)	
Ce–B	2.80 (× 2), 2.81(× 2)	2.69 (× 2), 2.87 (× 2)	

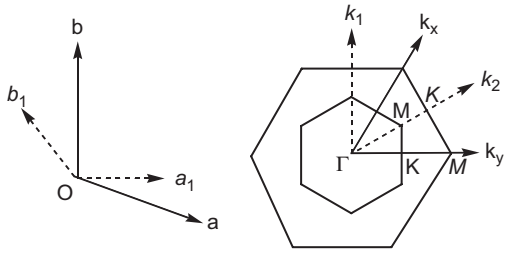

Fig. 3. Primitive cell (a_1, b_1) and $(\sqrt{3}\times\sqrt{3})R30^\circ$ supercell (a, b) (left) and primitive (k_1, k_1) and $(\sqrt{3}\times\sqrt{3})R30^\circ$ (k_x, k_y) Brillouin zones (right) for graphite.

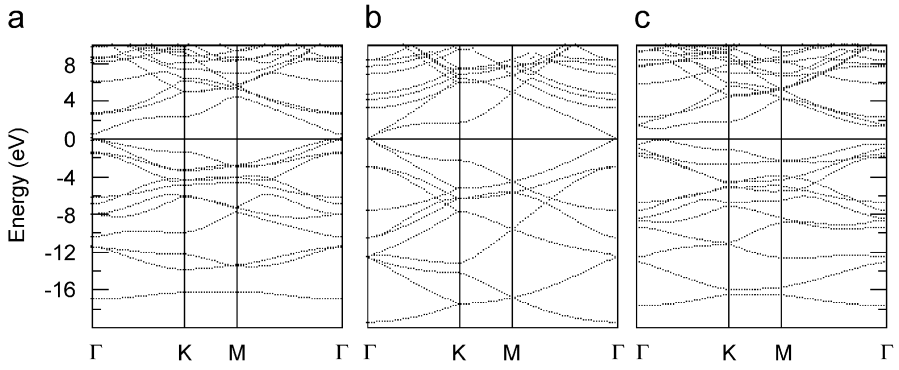

Fig. 2. Band structure of (a) $[B_2C_4]^{2-}$ (coloring **I**), (b) graphite, and (c) $[B_2C_4]^{2-}$ (coloring **II**), within the pseudo-hexagonal unit cells. A $(\sqrt{3}\times\sqrt{3})R30^\circ$ Brillouin zone is considered for graphite (see Fig. 3).

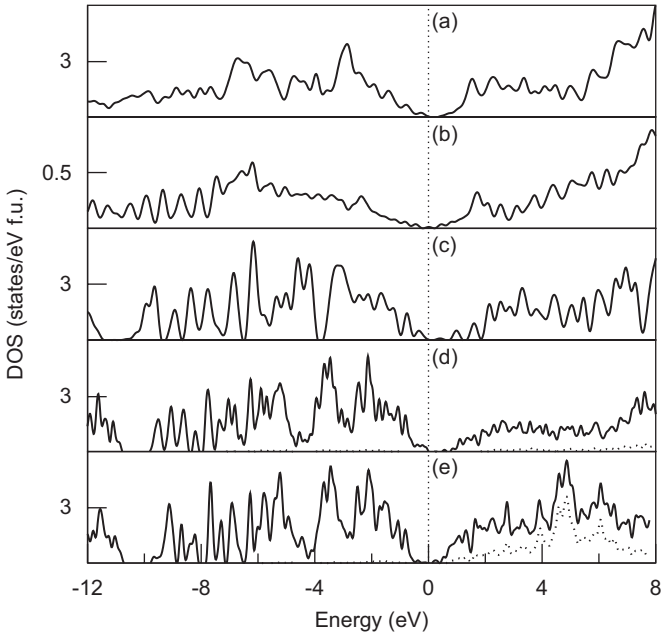

Fig. 4. DOS of (a) 2D $[B_2C_4]^{2-}$ (coloring **I**), (b) 2D graphite, (c) 2D $[B_2C_4]^{2-}$ (coloring **II**), (d) MgB_2C_4 (structure **Ib**), and (e) CaB_2C_4 (structure **Ib**). For MgB_2C_4 (d) the dotted line represents the contribution of Mg 3*s* and 3*p* states. For CaB_2C_4 (e) the dotted line represents the contribution of Ca ions.

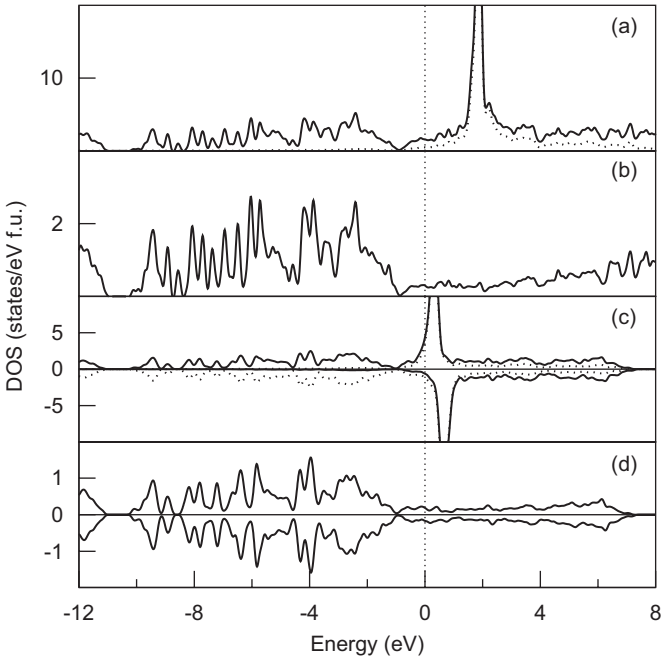

Fig. 5. DOS for LnB_2C_4 with structure **Ia**: (a) Total (solid line) and partial La 5*d* and 4*f* (dotted line) DOS of LaB_2C_4, (b) partial B_2C_4 DOS of LaB_2C_4, (c) total (solid line) and partial Ce 5*d* and 4*f* (dotted line) spin-polarized DOS of CeB_2C_4, and (d) partial B_2C_4 DOS of CeB_2C_4.

total DOS computed for MgB_2C_4 (Fig. 4d) and CaB_2C_4 (Fig. 4e) with the most energetically stable coloring **I** arrangement is very similar to that of the $[B_2C_4]^{2-}$ model (Fig. 4c). Both compounds are calculated to be semiconductors with a band gap of about 0.2 eV for the Mg compound and 0.4 eV for the Ca compound. Electron occupations of the Mg/Ca 3*s*/4*s*, 3*p*/4*p* orbitals after interactions with the boron–carbon sub-lattice are insignificant. Therefore, an ionic model is valid to describe the electronic properties of these two compounds.

A stronger covalent character between the metal atoms and the B/C sheets is computed with La or Ce. With Wigner–Seitz spheres of about 1.6 Å for La and Ce, integration of the electron density gives about 0.8 electrons per La/Ce in the La/Ce 5*d* orbitals. Furthermore, the 4*f* orbitals are empty for La and are occupied by about one electron for Ce. This seems to indicate that in these compounds, the metals essentially must act as two-electron donors with respect to the boron–carbon network B_2C_4, the other electrons remaining in the relatively narrow d band of the metals. This is illustrated in Fig. 5, which shows the DOS of LaB_2C_4 and CeB_2C_4. The Fermi level crosses a peak of density of states which is mainly metal in character. Interestingly, there is a pseudo band gap at about 0.9 eV below the Fermi level, which separates the π-bonding and the π^*-antibonding bands of the B_2C_4 sub-lattice in both compounds. Indeed, the DOS below the pseudo band gap (from about −16.5 eV to −0.9 eV) is highly comparable to that of the $[B_2C_4]^{2-}$ model below its Fermi level (compare Figs. 4b and the boron–carbon contribution in Fig. 5). Occupation of the states localized between this pseudo band gap and the Fermi level corresponds roughly to one electron. This clearly shows that this extra electron does not destabilize coloring **I** arrangement since identical B–C and C–C are computed for Mg, Ca, La and Ce metals. Indeed, the bottom of the partially occupied π^* bands of the B_2C_4 sub-lattice is weakly antibonding, mixing with the top of the bonding π bands of the B_2C_4 sub-lattice.

4. Conclusion

In summary, first-principles calculations were performed on the crystal structures of the ternary rare-earth metal carbon borides MB_2C_4 (M = Mg, Ca; La and Ce) using the DFT-GGA computational method. Structural optimisations and total energy calculations indicate that these compounds adopt a layered structure consisting of graphite-like B_2C_4 layers alternating with metal sheets. Within the hexagonal B/C layers, the coloring of the –C–C–C–B–C–B– sequence is energetically more favorable than that of the –C–C–C–C–B–B– sequence. The metal atom arrangements along the staking direction, either on top (structure **Ia**) of each other or in zigzag (structure **Ib**), are nearly iso-energetic, with a tiny preference for structure **Ib** with the alkaline-earth metals and for structure **Ia** with rare-earth metals. The electronic structures of these compounds, mainly determined by the B_2C_4 sheets, can be rationalized with the simple valence electron distribution $M^{2+}[B_2C_4]^{2-}$, with the metals essentially acting as two-electron donors with respect to the boron–carbon network, the other Ln valence electron remaining in the

relatively narrow d band of the metals. Accordingly, MB_2C_4 compounds are narrow-gap semi-conductors ($\Delta E \approx 0.2$ to 0.4 eV) with $M =$ Mg and Ca, but metallic in character with $M =$ La or Ce. The Fermi level is about 0.9 eV above a pseudo-gap between the bonding π and antibonding π^* states of the B/C atoms for $M =$ Ln. The Fermi level crosses a rather high peak of DOS of Ln 5d states admixed with some B/C π^* states.

5. Supplementary material

Optimized cell parameters and atomic fractional coordinates of different MB_2C_4 arrangements within the orthorhombic system are provided in Tables S1 and S2.

Acknowledgments

Thanks are expressed to the Institut de Développement et de Ressources en Informatique Scientifique (IDRIS-CNRS), and the Centre Informatique National de l'Enseignement Supérieur (CINES) for computing facilities. C.-M. Fang thanks the Centre National de la Recherche Scientifique (France) for a Visiting Scientist fellowship.

Appendix A. Supplementary material

Supplementary data associated with this article can be found in the online version at doi:10.1016/j.jssc.2007.06.028.

References

[1] J. Bauer, J.-F. Halet, J.-Y. Saillard, Coord. Chem. Rev. 178–180 (1998) 723 , and references therein.
[2] J.-F. Halet, in: M.G. Davidson, A.K. Hugues, T.B. Marder, K. Wade (Eds.), Contemporary Boron Chemistry, Royal Society of Chemistry, Cambridge, 2000, p. 514 , and references therein.
[3] M. Ben Yahia, J. Roger, X. Rocquefelte, R. Gautier, J. Bauer, R. Guérin, J.-Y. Saillard, J.-F. Halet, J. Solid State Chem. 179 (2006) 2779 , and references therein.
[4] F. Wiitkar, S. Kahlal, J.-F. Halet, J.-Y. Saillard, J. Bauer, P. Rogl, J. Am. Chem. Soc. 116 (1994) 251.
[5] L. Ya. Markovskii, N.V. Vekshina, G.F. Pron, Vysoko-temp. Neorgan. Soedin. Akad. Nauk Ukr. SSR, Inst. Probl. Materialoved (1965) 415.
[6] L. Ya. Markovskii, N.V. Vekshina, Zhurnal Prikladnoi Khimi (Saint-Petersburg Russian Federation) 37 (1964) 2126.
[7] J. Bauer, in: D. Emin, T. Aselage, A. C. Switendick, B. Morosin, C. L. Beckel (Eds.), Boron-Rich Solids, AIP Conference Proceedings, vol. 231, American Institute of Physics, New York, 1991, p. 216.
[8] J.K. Burdett, E. Canadell, T. Hughbanks, J. Am. Chem. Soc. 108 (1986) 3971;
For a general discussion on the coloring problem in solids see G.J. Miller, Eur. J. Inorg. Chem. (1998) 523.
[9] X. Rocquefelte, S.E. Boulfelfel, M. Ben Yahia, J. Bauer, J.-Y. Saillard, J.-F. Halet, Angew. Int. Ed. 44 (2005) 7542.
[10] C. M. Fang, S.-E. Boulfelfel, B. Le Guennic, L. Le Pollès, R. Gautier, J. Bauer, J.-Y. Saillard, J.-F. Halet, to be published.
[11] G. Kresse, J. Furthmuller, Phys. Rev. B 54 (1996) 11169.
[12] G. Kresse, J. Furthmueller, Comput. Mater. Sci. 6 (1996) 15.
[13] P.E. Blöchl, Phys. Rev. B 50 (1994) 17953.
[14] G. Kresse, J. Furthmüller, Phys. Rev. B 54 (1999) 1758.
[15] J.P. Perdew, S. Burke, M. Ernenrhof, Phys. Rev. Lett. 77 (1996) 3865.
[16] H.J. Monkhorst, J.D. Pack, Phys. Rev. B 13 (1976) 5188.
[17] M. Wörle, R. Nesper, J. Alloys Compd. 216 (1994) 75.
[18] M. Wörle, R. Nesper, G. Mair, M. Schwarz, H.G. Von Schnering, Z. Anorg. Allg. Chem. 621 (1995) 1153.
[19] See for example, R. Ahuja, S. Auluck, J. Trygg, J.M. Wills, O. Eriksson, B. Joansson, Phys. Rev. B, 51, 1995, 4813, and references therein.